Applied Catalysis B: Environmental 203 (2017) 541–548

Contents lists available at ScienceDirect

Applied Catalysis B: Environmental

journal homepage: www.elsevier.com/locate/apcatb

$Pt/C_{N\text{-doped}}$ electrocatalysts: Superior electrocatalytic activity for methanol oxidation reaction and mechanistic insight into interfacial enhancement

Gui-fa Long [a], Xiao-hua Li [a], Kai Wan [a], Zhen-xing Liang [a,*], Jin-hua Piao [c], Panagiotis Tsiakaras [b,d,**]

[a] Key Laboratory on Fuel Cell Technology of Guangdong Province, School of Chemistry and Chemical Engineering, South China, University of Technology, Guangzhou 510641, PR China
[b] Laboratory of Alternative Energy Conversion Systems, Department of Mechanical Engineering, School of Engineering, University of Thessaly, Pedion Areos, 38334 Volos, Greece
[c] School of Food Science and Engineering, South China University of Technology, Guangzhou 510641, PR China
[d] Laboratory of Electrochemical Devices based on Solid Oxide Proton Electrolytes, Institute of High Temperature Electrochemistry, Yekaterinburg 620990, Russia

ARTICLE INFO

Article history:
Received 15 July 2016
Received in revised form 11 October 2016
Accepted 18 October 2016
Available online 19 October 2016

Keywords:
Methanol oxidation reaction
Nitrogen-doped carbon
Pt nanoparticles
Non-poisoning ability

ABSTRACT

Nitrogen-doped ordered mesoporous carbon (NOMC) is studied as the support to synthesize a $Pt/C_{N\text{-doped}}$ catalyst for methanol oxidation reaction (MOR). The effects of carbon dimension and metal loading are investigated by nitrogen ad/desorption isotherms, transmission electron microscopy (TEM), X-ray diffraction (XRD), X-ray photoelectron spectroscopy (XPS) and electrochemical methods. Both TEM and XRD results show that platinum nanoparticles (Pt NPs) are highly dispersed on NOMC with a uniform and narrow distribution, while the dimension of NOMC has a considerable effect on the dispersion of Pt. For 10 wt% metal loading, the average diameter of Pt NPs on 2D-NOMC is 1.40 nm; smaller than that on 3D-NOMC (1.90 nm). XPS results reveal that a strong electronic interaction exists between Pt and NOMC, indicating the formation of Pt–N bonds at the interface. Such an interaction gets more pronounced in the case of low Pt loadings and low-dimensional supports; the reason is that the 2D support is more accessible to load Pt and the metal-support interface is better developed at low metal loadings.

The electrochemical results are well correlated with the physiochemical characterizations. 1) The electrochemically active surface area of Pt is higher on the 2D-support than that on the 3D-one, confirming the better dispersion of Pt on NOMC-2D. 2) A positive shift in the potential is observed for the adsorption of oxygen-containing species onto Pt, which is indicative of the charge transfer from Pt to the support and the formation of Pt–N bonds. 3) Both onset and peak potentials are negatively shifted by *ca.* 50 mV for MOR on 10 wt% Pt/NOMC-2D, as compared with the commercial Pt/XC-72. The ratio of forward to backward current, a measure of poisoning tolerance, is 1.1 on Pt/NOMC-2D and 0.80 on Pt/XC-72R. This enhancement can be attributed to the bifunctional mechanism at the $Pt/C_{N\text{-doped}}$ interface. In MOR, CO-like intermediate species on Pt can be effectively stripped off by the adjacent active –OH species on carbon, generated at lower potentials.

1. Introduction

In the last decade, the direct methanol fuel cell (DMFC) has been extensively studied as it shows a promise in electronic applications [1]. The DMFC offers many advantages, such as the fast fuel charging, simple operation, and high energy density; however, there are still a number of issues left to be resolved. First, its cost is too high as the noble metal Pt catalyst is required and its usage is high up to 6 mg cm^{-2} [2–7]. Second, the performance does not meet the

* Corresponding author at: Key Laboratory on Fuel Cell Technology of Guangdong Province, School of Chemistry and Chemical Engineering, South China, University of Technology, Guangzhou 510641, PR China.
** Corresponding author at: Laboratory of Alternative Energy Conversion Systems, Department of Mechanical Engineering, School of Engineering, University of Thessaly, Pedion Areos, 38334 Volos, Greece and Laboratory of Electrochemical Devices based on Solid Oxide Proton Electrolytes, Institute of High Temperature Electrochemistry, Yekaterinburg 620990, Russia.
E-mail addresses: zliang@scut.edu.cn (Z.-x. Liang), tsiak@uth.gr (P. Tsiakaras).

http://dx.doi.org/10.1016/j.apcatb.2016.10.055
0926-3373/

requirement of practical application due to the slow kinetics of the methanol oxidation reaction (MOR) and the oxygen reduction reaction (ORR) on the current Pt catalyst [8–11]. To address these issues, it is highly desirable to increase the specific activity of Pt and its anti-poisoning ability against CO-like intermediate species in the MOR.

Carbon black powders (like Vulcan XC-72R, BP-2000) are commercially used as the support to increase the dispersion and specific activity of Pt [12,13]. Recently, nanostructured carbons, like carbon nanotube [14–16], carbon nanofiber [17,18], graphene [19], which are featured by either high electronic conductivity or specific surface area, have been explored to support the Pt nanoparticles (Pt NPs) [20]. Among them, ordered mesoporous carbon (OMC) features an extremely high specific surface area and ordered mesoporous pore structure, which favors the dispersion of Pt and the mass transfer in the porous electrode [21–24]. In particular, nitrogen-doped ordered mesoporous carbon (NOMC) has a variety of enriched 'electrochemically active' functional groups on the surface, which is thereby highly promising in the application of the electrochemical energy technologies [25–27]. The doping of nitrogen yields considerable effects on carbon by adjusting the electronic/geometric structure, the basicity and the hydrophilicity. Such an activation of carbon facilitates the nucleation, growth, loading and anchoring of Pt NPs [28,29]. As such, NOMC is expected to be an effective support and capable of highly dispersing and stabilizing the Pt NPs. Besides, the dopant N atoms can denote charge to the adjacent atoms and thus results in strong metal-support interaction (SMSI) at the interface, yielding a considerable effect on both the activity and durability of the catalyst[30–32]. By using the nitrogen-doped carbon support [1,33–35], the Pt/C catalyst shows a significant enhancement in the activity for the oxidation of methanol [36–40] and glycerol [41]. Very recently, it is found that NOMC, as a metal-free electrocatalyst, shows a decent electrocatalytic activity to the oxygen reduction reaction (ORR) and hydrogen evolution reaction (HER) [42–44].

In terms of the synthesis, NOMC is generally obtained by the nanocasting method, in which the ordered mesoporous silica (OMS), like SBA-15, is used as the hard template. As such, the synthesized NOMC is the reverse replica of the template. It is reported that SBA-15 is in the column-like morphology, of which the diameter is several hundred nanometers and the length is several microns [25,45–52]. It is understandable that both the deposition of Pt NPs and the MOR are not easy to proceed in such long-range mesopores due to the mass transfer issues. Therefore, the above-mentioned morphological features seriously limit NOMC as the support to disperse and anchor the Pt NPs. As a result, the interface of Pt/NOMC is not well developed and, the enriched electrochemically active functional groups on carbon cannot be fully utilized to promote the activity and durability.

To address this issue, a 2D nitrogen-doped ordered mesoporous carbon (NOMC-2D) is developed as the support in this work. The Pt NPs are loaded onto the nitrogen-doped carbon with either 2D- or 3D-morphology for comparison. The physiochemical characterizations reveal that there exists a stronger interaction between the metal and the support in Pt/NOMC-2D than Pt/NOMC-3D, and the metal-support interface is better developed in the former one. The electrochemical result suggests that the nitrogen-doped carbon support indeed improves both the electrocatalytic activity and the anti-poisoning ability of Pt for the MOR than does the carbon black (Vulcan XC-72R). The enhancement can be understood as a result of the bifunctional mechanism at the interface of Pt-$C_{N\text{-doped}}$. That is, the enriched electrochemically active −OH groups on carbon help to strip off the CO-like intermediate species adsorbed on the adjacent Pt atoms. This mechanism is verified by the extensive investigation on both the loading of Pt and the dimension of the carbon support. The 10 wt% Pt/NOMC-2D catalyst yields the lowest overpotential and highest anti-poisoning ability as more bifunctional active sites are generated at the interface.

2. Experimental

2.1. Preparation of NOMC-3D and NOMC-2D

3D nitrogen-doped ordered mesoporous carbon (NOMC-3D) was synthesized by the nanocasting method [25–27], using SBA-15 as the hard template and 1, 10-phenanthroline monohydrate ($C_{12}H_8N_2{\cdot}H_2O$) as the precursor. First, the $C_{12}H_8N_2{\cdot}H_2O$ was dissolved into ethanol and mixed with the $FeCl_2{\cdot}4H_2O$ aqueous solution. Second, the SBA-15 template was added in and sonicated at room temperature. Then, the product was filtrated, washed, dried, and then pyrolysed at 900 °C in argon (99.999%). Finally, NOMC-3D was obtained by removing the silica template and iron by successively boiling the powders in 10 M NaOH at 120 °C and 0.10 M $HClO_4$ at 80 °C for 24 h.

2D nitrogen-doped ordered mesoporous carbon (NOMC-2D) was synthesized by the same procedure to NOMC-3D, except the use of a 2D silica template. The synthesis of 2D silica is as follows [53]. i) Graphene oxide (GO) was dispersed in a mixture of 126 ml deionized (DI) water and 20 ml hydrochloric acid (37 wt%), and then P123 was added in as the organic template. ii) 9.2 ml tetraethyl orthosilicate (TEOS) was added in and stirred for 20 h at 35 °C, which was hydrothermally treated at 110 °C for 12 h. iii) The product was filtered and microwave-digested in the mixture of HNO_3 and H_2O_2 to remove the organic template.

2.2. Preparation of Pt/NOMC

Pt nanoparticles (Pt NPs) were loaded on NOMC by the aid of ethylene glycol (EG) reduction method [54]. 250 mg NOMC was suspended in 25 ml EG under ultrasonic stirring for 40 min. A given amount of the H_2PtCl_6/EG solution (Pt: 3.7 mg mL^{-1}) was added in order to obtain Pt/NOMC with two metal loadings: 10 wt% and 30 wt%. Then, the pH of the solution was adjusted to 13 by adding NaOH and heated at 130 °C for 3 h under flowing Ar. After cooling down to the room temperature, the pH of the mixture was adjusted to 2 by adding 1.0 M HCl aqueous solution, which was stirred for another 2 h to ensure that Pt NPs were fully loaded on NOMC. Finally, the powders were filtrated, washed and dried at 80 °C for 8 h in vacuum oven.

2.3. Physicochemical characterization

X-ray diffraction (XRD) measurements were carried out by using a TD-3500 X diffractometer (Tongda Technology, China) with a Cu Kα radiation source operated at 40 keV and at a scan rate of 0.05 s^{-1}. X ray photoelectron spectroscopy (XPS) measurement was carried out with a physical Electronics PHI 5600 multi-technique system using an Al monochromatic X-ray at a power of 350 W. Transmission electron microscopy (TEM) images were collected on a FEI Tecnai G2 F20 S-TMIN operated at 200 kV. Thermogravimetric analyses (TGA) were made using a TA Instrument SDT 2960. The experiment was performed at 10 °C min^{-1} from room temperature to 800 °C in air at a flow rate of 20 ml min^{-1}. Nitrogen adsorption/desorption isotherms were measured at 77 K using Micromeritics TriStar II 3020 analyzer. The total surface area was analyzed with the well-established Brunauer-Emmer-Teller (BET) method, the microporous (MP) surface area was obtained with the *t*-plot method, and the pore size distribution was analyzed by the Barrett-Joyner-Halenda (BJH) method.

2.4. Electrochemical characterization

The electrochemical behavior of the catalyst was characterized by the cyclic voltammetry (CV) using a three-electrode cell with electrochemical work station of Zennium (Zahner) at room temperature (25 °C). A platinum wire and a saturated calomel electrode (SCE) were used as the counter and reference electrodes, respectively. The working electrode was a glassy carbon disk (5.0 mm in diameter, PINE) covered with a thin layer of Nafion-impregnated catalyst. Typically, the thin-film electrode was prepared as follows: 6.0 mg of the catalyst was dispersed in 0.60 ml Nafion/ethanol (0.84 wt% Nafion) and 3.40 ml ethanol by the sonication for 30 min. Then, a suitable volume of catalyst dispersion was transferred onto the glassy carbon disk by using a pipette and dried in room temperature. The Pt loading on the electrode was 15.3 $\mu g\,cm^{-2}$.

The electrolyte solution, 0.10 M $HClO_4$, was first bubbled with argon for 60 min. Then, the blank cyclic voltammograms were collected at 20 mV s^{-1} in the potential range between −0.27 and 0.88 V (vs. SCE) for 20 cycles. To evaluate the electrocatalytic activity of the MOR, the cyclic voltammograms were recorded in an aqueous solution containing 0.50 M CH_3OH + 0.10 M $HClO_4$. Then, the electrochemical signal of the MOR was extracted by subtracting the blank cyclic voltammogram. The reason for the subtraction is that carbon yields a considerable capacitive current in the supporting electrolyte (see Fig. S3); this current originates from both the double layer capacitance and pseudocapacitance, which basically remains unchanged for all solutions. As such, this current can be seen as a background one, which can be subtracted to better differentiate the faradaic current of MOR.

The CO stripping voltammograms were collected as follow: 1) argon was bubbled into 0.10 M $HClO_4$ for 60 min and the blank CVs were collected, 2) CO was bubbled for 30 min to allow saturated adsorption of CO on the catalyst while maintaining the potential at 0.05 V vs. SCE, 3) argon was purged for 30 min to remove the dissolved CO in the electrolyte while maintaining potential at 0.05 V vs. SCE, 4) the potential was scanned from the 0.05 to 0.88 V at 20 mV s^{-1}, to record the voltammograms for two cycles.

3. Results and discussion

Fig. 1 shows the TEM images and the particle size distribution histograms of the following six catalysts: 10 wt% Pt/NOMC-3D, 10 wt% Pt/NOMC-2D, 10 wt% Pt/XC-72 (ETEK), 30 wt% Pt/NOMC-3D, 30 wt% Pt/NOMC-2D, and 30 wt% Pt/XC-72 (ETEK). Figs. 1a-1c reveal that Pt NPs are uniformly dispersed on the surface of the carbon support, and the average diameter is close to 1.90, 1.40, 2.01 nm respectively for the three former catalysts, loaded with 10 wt% of Pt. It is thus inferred that the nitrogen-doped carbon (NOMC), as the support, yields a narrower size distribution (see Figs. 1a'-c') and better dispersion of the Pt NPs than does XC-72. This trend becomes clearer at the higher loading of 30 wt%. Figs. 1d-f intuitively confirm more serious agglomeration of Pt NPs on XC-72 than on the two NOMCs. The average diameter in this case is 2.53, 2.31 and 3.19 nm respectively for the three latter catalysts, loaded with 30 wt% Pt. The better dispersion of Pt NPs on NOMC can be explained as follows: i) the specific surface area of NOMC is much larger than that of XC-72 (see Table S1) and ii) the dopant nitrogen atoms can interact with the metal atoms, favoring the nucleation and loading of the Pt NPs.

It is noted that the dispersion of Pt is also different on the two NOMC supports. The surface area of NOMC-2D is smaller than that of NOMC-3D; however, the size of Pt NPs is much smaller on the former support. It is thus inferred that the characteristic dimension of the carbon support yields a considerable effect on Pt NPs.

Such a difference should originate from the 'accessible' surface as the support. The NOMC-3D particle is in 'block' (μm-scale) morphology (see Fig. S1a) associated with long-range mesopores, and the surface area is mainly contributed by these mesopores. It is understandable that the deposition of Pt NPs will be seriously inhibited onto the inner walls of the 'deep' pores considering the mass transfer issue. As such, the mesoporous surface cannot be fully used to disperse the active component, and therefore, Pt NPs preferentially deposit onto the outer surface of the carbon particles. In comparison, NOMC-2D is a film-like support with an ultrathin thickness of several nanometers (see Fig. S1b), in which the surface is available to support the Pt NPs. The above findings indicate that NOMC-2D, as the support, yields a stronger interaction with Pt than do the other two carbon materials.

Table 1
Content of each nitrogen containing component (%) of the Pt/$C_{N\text{-doped}}$ catalysts.

Sample	Pyridinic-N	Metal-N	Graphitic-N	Oxide-N
10 wt% Pt/NOMC-3D	29.78	8.99	50.45	10.78
10 wt% Pt/NOMC-2D	34.28	22.70	35.13	7.80
30 wt% Pt/NOMC-3D	35.37	12.59	39.94	12.10
30 wt% Pt/NOMC-2D	31.03	24.00	37.75	7.22

Fig. 2 depicts the XRD patterns of the catalysts. For all of them diffraction peaks appear at 39, 46, and 67°, and respectively correspond to (111), (200), and (220) facets of Pt (fcc) crystal.

As one can distinguish from Fig. 2a, the diffraction peaks are seriously broadened for the NOMC-loaded catalysts, as compared with the Pt/XC-72. This result indicates that for Pt/NOMC, the size of the Pt nanocrystallite is much smaller than that of Pt/XC-72, which agrees well with the TEM observation. For Pt/NOMC-3D, it is seen that the peak is sharpened with increasing the Pt loading, indicating that the crystallites tend to agglomerate; in comparison, for Pt/NOMC-2D, the broad peak basically remains unchanged at the two loadings. This result confirms that NOMC-2D is more effective as support, concerning the dispersion of the active Pt component.

XPS was used to investigate the surface composition (Table S2) and the electronic interaction between Pt and the support. Fig. 3 shows the high-resolution N 1s spectra. Figs. 3a–b present the N 1s spectra of two supports: NOMC-3D and NOMC-2D. It is seen that the shape of the curve varies significantly with the carbon support; in comparison, with the same support, the shape remains unchanged when increasing the Pt loading from 10 to 30 wt% (Figs. 3a & c).

To better describe the difference, the N 1s peak is deconvoluted based on four chemical states, *viz.* pyridinic-, metal coordinated-, graphitic-, and oxide-nitrogen [31]. The content of each component is calculated and shown in Table 1.

The most distinct feature is that the content of metal coordinated nitrogen (Pt-N) is much higher on NOMC-2D than NOMC-3D. This result can be understood as follows: i) firstly, the dopant nitrogen increases both the hydrophilicity and the eletrophilicity of the carbon support, which thereby promotes the nucleation and anchoring of the Pt NPs, ii) secondly, the 2D support effectively extends its accessible interface with the Pt NPs, yielding a higher content of Pt-N. Such an interaction is further evidenced by the shift in the binding energy of Pt 4f peak, as shown below.

Fig. 4 shows the high-resolution Pt 4f spectra. It is seen that the carbon support indeed has a significant effect on the chemical state of Pt, which is indicative of the strong electronic interaction between them. To quantify the difference, the peak is deconvoluted into three pairs of doublets (Pt^{00}, Pt^{2+}, Pt^{4+}) and, the results are below listed in Table 2.

It is seen that the binding energy of each peak follows the order of Pt/XC-72 < Pt/NOMC-3D < Pt/NOMC-2D. For example, the binding energy of $Pt^{00}4f_{7/2}$ is respective to 71.47, 71.54 and 71.64 eV for 10 wt% Pt/XC-72, Pt/NOMC-3D and Pt/NOMC-2D. The same trend is further seen for other peaks at the two Pt loadings, which confirms the formation of the aforementioned Pt–N bond at the interface. In

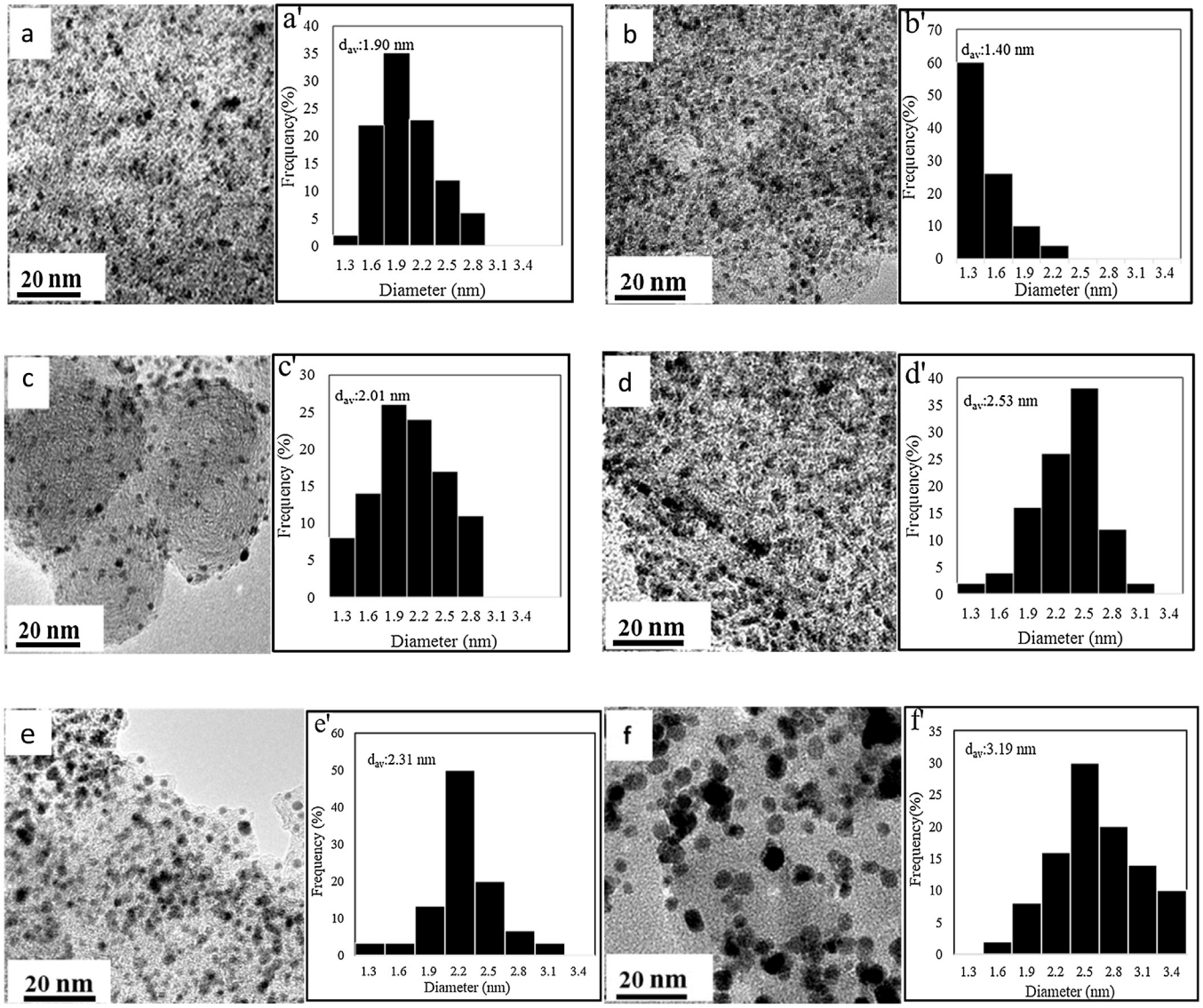

Fig. 1. TEM images (left) and particle size distribution histograms (right) of the Pt-base catalysts: (a, a') 10 wt% Pt/NOMC-3D, (b, b') 10 wt% Pt/NOMC-2D, (c, c') 10 wt% Pt/XC-72, (d, d') 30 wt% Pt/NOMC-3D, (e, e') 30 wt% Pt/NOMC-2D, and (f, f') 30 wt% Pt/XC-72.

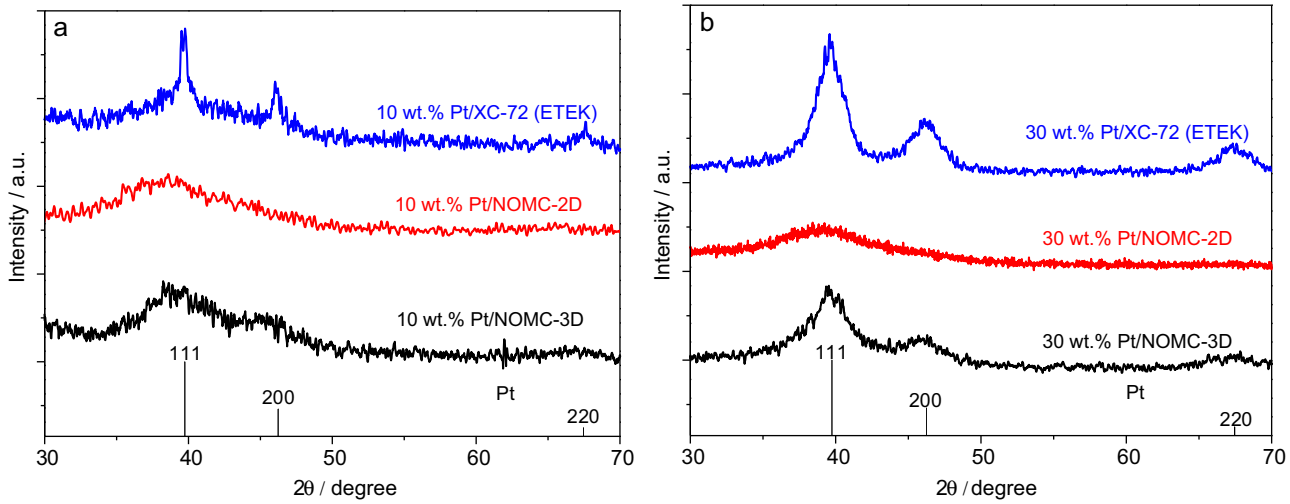

Fig. 2. XRD patterns of the synthesized Pt catalysts and the commercial Pt catalysts: (a) 10 wt% Pt/C and (b) 30 wt% Pt/C.

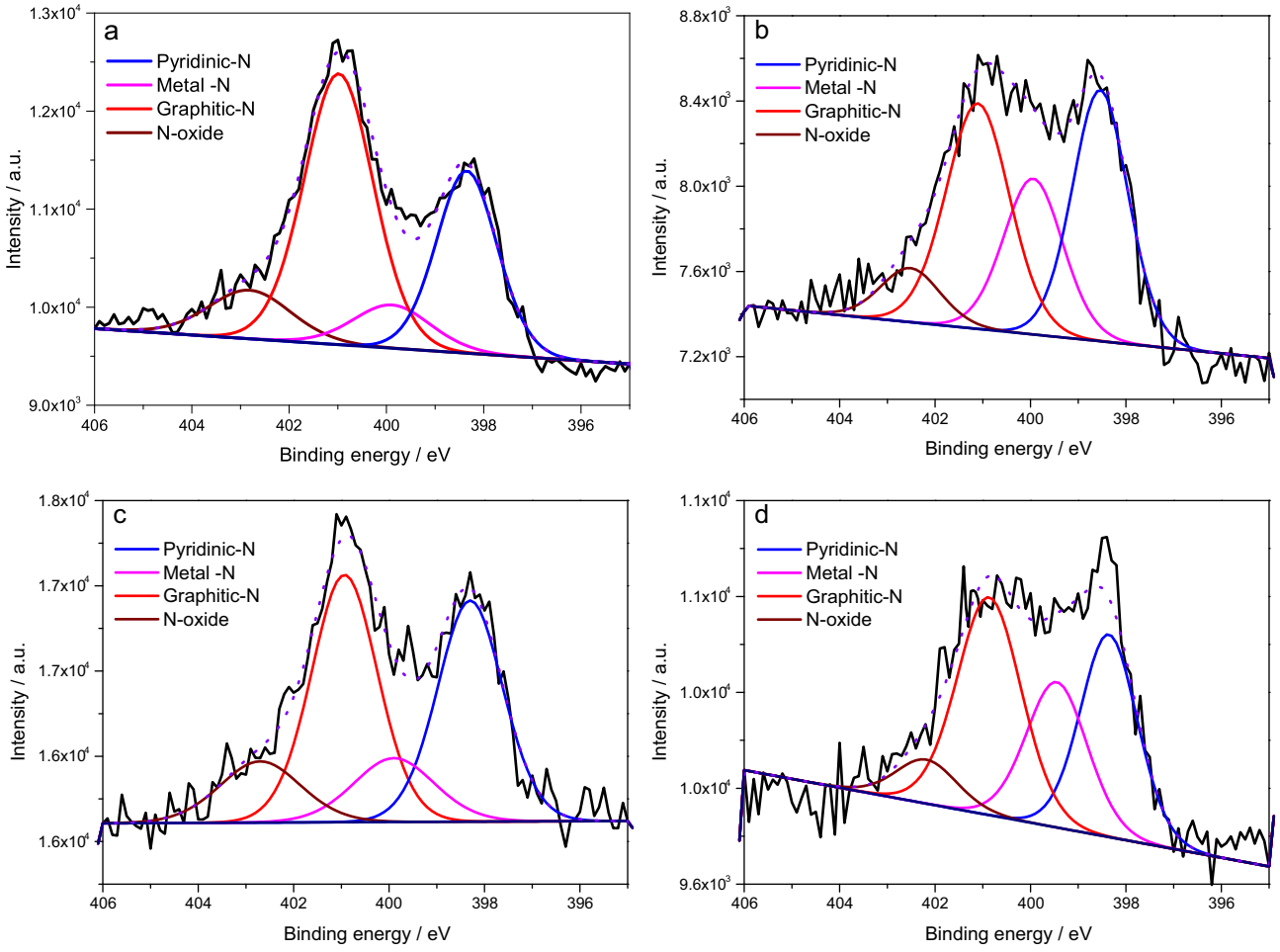

Fig. 3. N 1 s XPS spectra: (a) 10 wt% Pt/NOMC-3D, (b) 10 wt% Pt/NOMC-2D, (c) 30 wt% Pt/NOMC-3D, and (d) 30 wt% Pt/NOMC-2D.

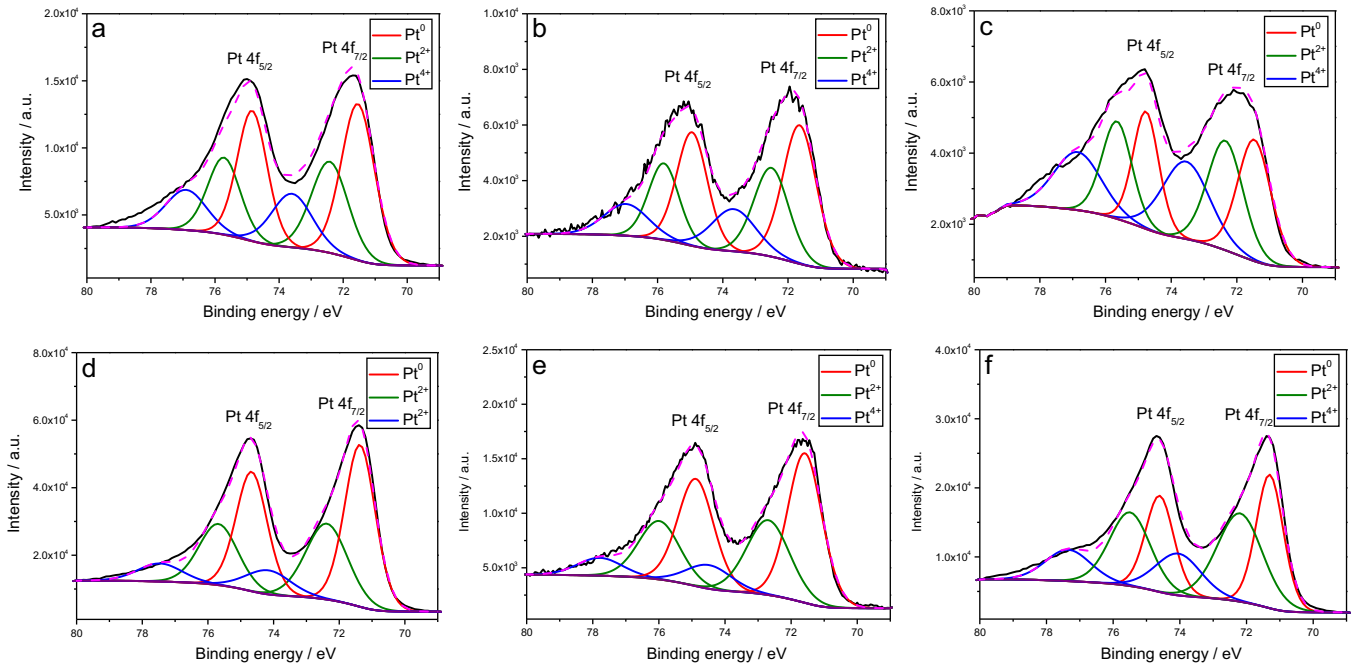

Fig. 4. Pt 4f XPS spectra: a) 10 wt% Pt/NOMC-3D, b) 10 wt% Pt/NOMC-2D, c) 10 wt% Pt/XC-72, d) 30 wt% Pt/NOMC-3D, e) 30 wt% Pt/NOMC-2D, and f) 30 wt% Pt/XC-72.

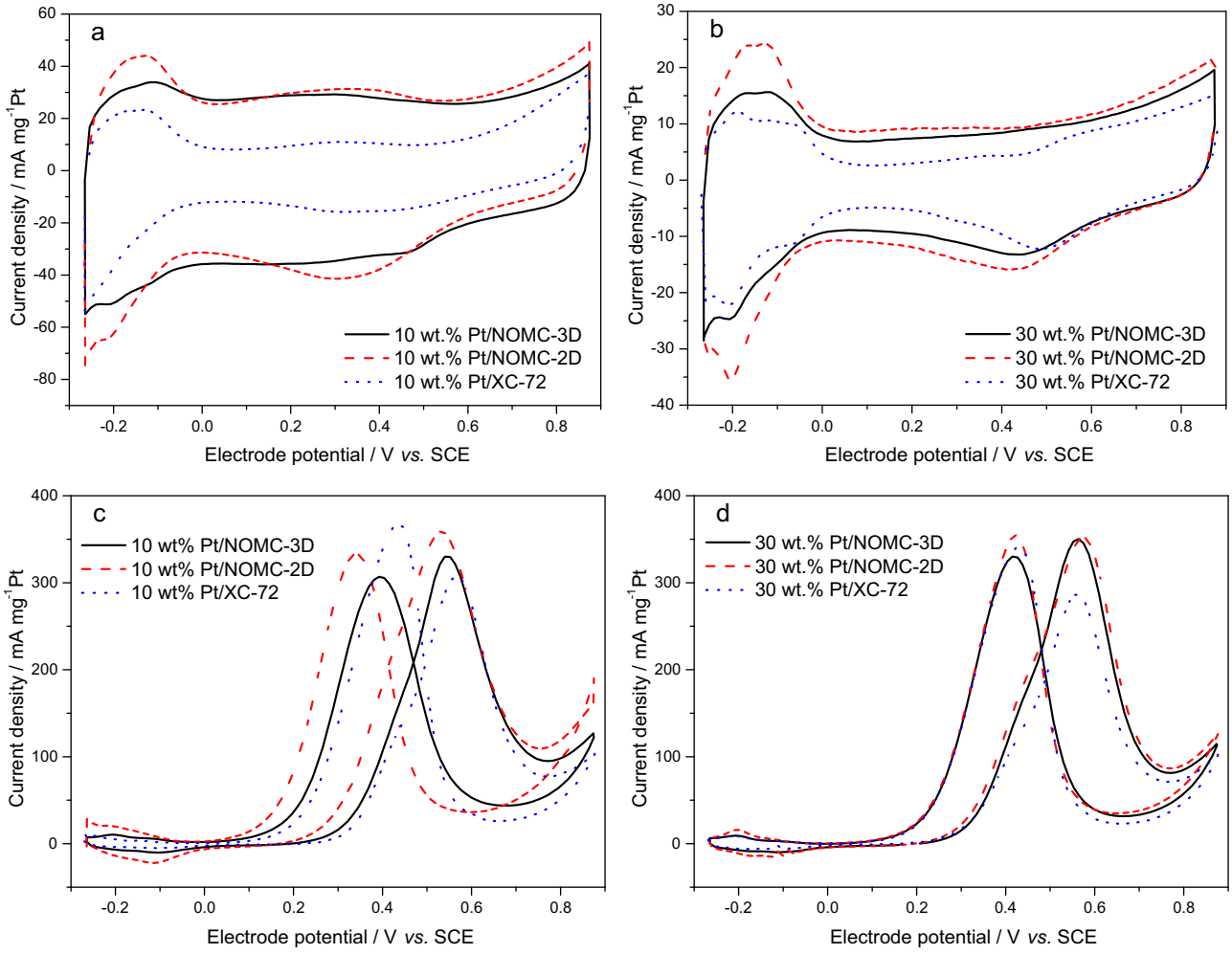

Fig. 5. Cyclic voltammograms of 10 wt% Pt/C and 30 wt% Pt/C collected at a scan rate of 20 mV s^{-1} at room temperature in the following solutions: (a, b) 0.10 M $HClO_4$ (a, b), and (c, d) 0.50 M CH_3OH + 0.10 M $HClO_4$ (background-corrected).

Table 2
Content of each platinum component (%) of the following catalysts: a) 10 wt% Pt/NOMC-3D, b) 10 wt% Pt/NOMC-2D, c) 10 wt% Pt/XC-72, d) 30 wt% Pt/NOMC-3D, e) 30 wt% Pt/NOMC-2D, f) 30 wt% Pt/XC-72.

		a	b	c	d	e	f
$Pt^0 4f_{7/2}$	BE/eV	71.54	71.64	71.47	71.37	71.58	71.30
$Pt^0 4f_{5/2}$	BE/eV	74.84	74.94	74.77	74.67	74.88	74.60
	Content/%	48.49	48.33	34.83	53.94	54.74	38.15
$Pt^{2+} 4f_{7/2}$	BE/eV	72.42	72.51	72.35	72.38	72.69	72.20
$Pt^{2+} 4f_{5/2}$	BE/eV	75.72	75.81	75.65	75.68	75.99	75.50
	Content/%	31.19	32.29	33.54	34.42	34.24	41.97
$Pt^{4+} 4f_{7/2}$	BE/eV	73.60	73.67	73.55	74.16	74.48	74.05
$Pt^{4+} 4f_{5/2}$	BE/eV	76.90	76.97	76.85	77.46	77.78	77.35
	Content/%	20.32	19.38	31.63	11.64	11.29	19.88

summary, XPS gives the direct evidence for the electronic interaction between the active component and the nitrogen-doped carbon support, favoring the dispersion of the Pt NPs. As shown below, such an interaction further yields some effect on the electrochemical behavior.

Fig. 5 depicts the cyclic voltammograms of the catalysts in both blank electrolyte and the methanol-containing electrolyte.

From Figs. 5a–b, a much higher capacitive current is seen for Pt/NOMC than Pt/XC-72, which can be attributed to the larger specific surface area of NOMC. Also, the nitrogen-doped carbon has a variety of enriched electrochemically active functional groups, of which the electrochemical transition generates a high pseudocapacitive current [55].

Moreover, the characteristic peaks of Pt are seen in the investigated potential range. The cathodic and anodic peaks between −0.27 and 0.1 V are due to the adsorption and desorption of hydrogen on Pt [56]. The electrochemical active surface area (ECSA) of Pt is thus calculated and listed in Table 3.

At the Pt loading of 10 wt%, NOMC-2D yields a much larger $ECSA_H$ than XC-72 does, which is due to the higher dispersion of the former catalyst. This result agrees well with the TEM and XRD results. It is noted that, albeit the higher dispersion, Pt/NOMC-3D shows a smaller $ECSA_H$ than does Pt/XC-72. This seeming inconsistency originates from the inappropriate subtraction of the capacitive current, which is not well defined in the potential range. The current at *ca.* 0 V should not be used as the background, as the hydrogen spillover may occur at the interface of Pt/NOMC. This phenomenon relies on the amount of the interfacial atoms, which gets more pronounced at a low Pt loading (10 wt%) but lessened at the high loading (30 wt%). As such, the estimation of $ECSA_H$ may be misleading by using the underpotential deposition of hydrogen. Herein, the ECSA was re-analyzed from the CO-stripping results (see Fig. 6), as listed in Table 3. For the two Pt loadings, the $ECSA_{CO}$ follows the ordered: XC–72 < NOMC-3D < NOMC-2D, which correlates well with the above analysis.

It should be noted that the anodic current above 0.5 V is attributed to the adsorption of oxygen-containing species on Pt.

Table 3
The electrochemical parameters of the Pt catalysts.

Sample	$ECSA_H/m^2\ g^{-1}$	$ECSA_{CO}/m^2\ g^{-1}$	$I_f/mA\ mg^{-1}$	$I_b/mA\ mg^{-1}$	I_f/I_b
10 wt% Pt/NOMC-3D	40.2	85.1	331	307	1.1
10 wt% Pt/NOMC-2D	79.7	119.2	360	334	1.1
10 wt% Pt/XC-72	74.8	73.0	306	367	0.80
30 wt% Pt/NOMC-3D	45.8	72.3	351	331	1.1
30 wt% Pt/NOMC-2D	63.5	83.4	351	353	1.0
30 wt% Pt/XC-72	53.2	48.7	286	340	0.80

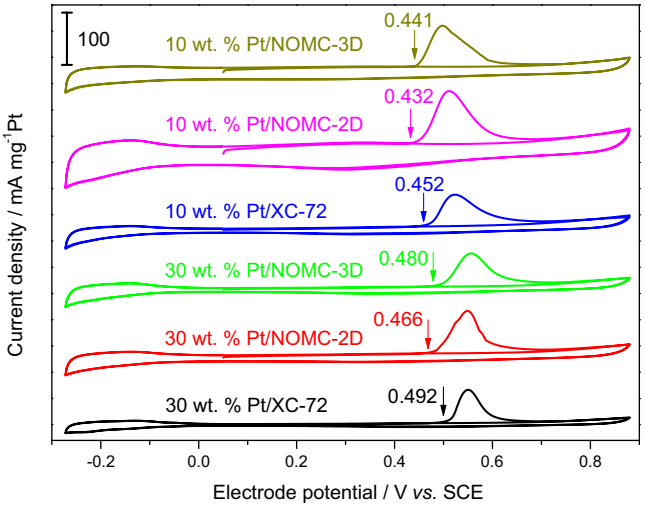

Fig. 6. CO stripping voltammograms of the catalysts collected at a scan rate of 20 mV s^{-1} at room temperature in 0.10 M $HClO_4$.

The onset potential shows a slight positive shift on NOMC compared with XC-72. This indicates that the charge is transferred from Pt to the support (e.g. dopant N), which is consistent with the XPS analysis [38].

The electrocatalytic activity is evaluated by using methanol as the probe molecule, as seen in Figs. 5c–d.

The peak potential of the NOMC-loaded catalysts (Fig. 5c) is much lower than that of Pt/XC-72. More specifically, among the three catalysts, Pt/NOMC-2D exhibits the lowest onset and peak potentials, which is also the best-performed catalyst when compared with the results in open literature (see Table S4). Therefore, it is concluded that the electrocatalytic activity can be significantly enhanced by using NOMC as the support. Such an enhancement can be attributed to both the better dispersion of the Pt NPs and the easier mass transfer in the ordered mesoporous carbon support. Furthermore, as mentioned above, Pt/NOMC-2D presents an extended interface between the active component and the support. At the interface, the oxygen-containing species on nitrogen-doped carbon can strip off the CO-like intermediate species adsorbed on the adjacent Pt atoms by the bifunctional mechanism [57], and, thereby lower its overpotential for the MOR [58].

This speculation is evidenced by the following results. The ratio of the forward current to the backward one, I_f/I_b (see Table 3), is indicative of the anti-poisoning ability against the CO-like intermediate species [59]. The ratio is 0.8 and 1.1 for Pt/XC-72 and Pt/NOMC, respectively. Fig. 6 shows the CO stripping voltammograms of the catalysts. It is seen that the onset potential of the CO_{ad} oxidation reaction follows the order: 10 wt% Pt/NOMC-2D (0.432 V) < 10 wt% Pt/NOMC-3D (0.441 V) < 10 wt% Pt/XC-72 (0.452 V) < 30 wt% Pt/NOMC-2D (0.466 V) < 30 wt% Pt/NOMC-3D (0.480 V) < 30 wt% Pt/XC-72 (0.493 V). This trend is a direct evidence for the anti-poisoning ability conferred by the support. At the same loading, NOMC-2D support is more effective to strip off the adjacent CO adsorbed on Pt than NOMC-3D and XC-72, as discussed above. Finally, as the Pt loading increases to 30 wt%, the size of Pt NPs increases; and consequently, the interfacial effect and the enhancement get less pronounced. Fig. 5d confirms this analysis, from which it is seen that the onset potential is similar for all the three catalysts.

4. Conclusions

The $Pt/C_{N\text{-doped}}$ catalyst was synthesized by using 2D nitrogen-doped carbon as the support. The as-prepared catalysts exhibited a superior electrocatalytic activity and non-poisoning ability for the reaction of methanol oxidation.

It is suggested that both nitrogen doping and 2D structure contribute to the enhancement of MOR electrocatalysis. The presence of dopant nitrogen yields a strong electronic interaction with Pt, which favors the dispersion and anchoring of Pt NPs. The 2-dimensional support can effectively extend the $Pt/C_{N\text{-doped}}$ interface, especially at a low Pt loading. At the interface, the enriched electrochemically active −OH groups on carbon help strip off the CO-like species on the adjacent Pt atoms. As such, the enhancement originates from the bifunctional mechanism conferred by the Pt/NOMC interface. The low-dimensional nitrogen-doped carbon is very promising to be used as both the co-catalyst and support in developing multi-functional catalysts.

In conclusion, this work does not only shed light on the interfacial electrocatalysis of the $Pt/C_{N\text{-doped}}$ for the MOR, but also help to guide the rational design of multifunctional electrocatalysts for fuel cells.

Acknowledgements

The work described in this paper was jointly supported by the National Natural Science Foundation of China (Nos. 21476087, 21576101, 21676106), National Key Research and Development Plan (No. 2016YFB0101200), Innovation Project of Guangdong Department of Education (No. 2014KTSCX016) and the Fundamental Research Funds for the Central Universities. Prof. Tsiakaras is also grateful to the "Bilateral R&D Cooperation program between Greece-China 2012–2014" and the Ministry of Education and Science of the Russian Federation (Mega-Grant, contract no. 14.Z50.31.0001) for funding.

Appendix A. Supplementary data

Supplementary data associated with this article can be found, in the online version, at http://dx.doi.org/10.1016/j.apcatb.2016.10.055.

References

[1] T. Maiyalagan, B. Viswanathan, U.V. Varadaraju, Electrochem. Commun. 7 (2005) 905–912.
[2] H. Huang, X. Wang, J. Mater. Chem. A 2 (2014) 6266–6291.
[3] X.X. Yan, Z.K. Tang, X. Xu, F. Fang, D.S. Song, J.G. Liu, S.F. Lu, L.M. Liu, J. Luo, J. Zhu, Nano Energy 21 (2016) 265–275.
[4] J. Xie, Q.H. Zhang, L. Gu, S. Xu, P. Wang, J.G. Liu, Y. Ding, Y.F. Yao, C.W. Nan, M. Zhao, Y. You, Z.G. Zou, Nano Energy 21 (2016) 247–257.

[5] P. Zhang, J.S. Lian, Q. Jiang, Phys. Chem. Chem. Phys. 14 (2012) 11715–11723.
[6] A.Q. Zhao, J. Masa, W. Schuhmann, W. Xia, J. Phys. Chem. C 117 (2013) 24283–24291.
[7] U. Tylus, Q. Jia, K. Strickland, N. Ramaswamy, A. Serov, P. Atanassov, S. Mukerjee, J. Phys. Chem. C 118 (2014) 8999–9008.
[8] Y. Kang, C.B. Murray, J. Am. Chem. Soc. 132 (2010) 7568–7569.
[9] Y. Xu, Y. Yuan, A. Ma, X. Wu, Y. Liu, B. Zhang, ChemPhysChem 13 (2012) 2601–2609.
[10] Z.X. Liang, T.S. Zhao, J.B. Xu, J. Power Sources 185 (2008) 166–170.
[11] J. Tang, T. Wang, X.C. Pan, X. Sun, X.L. Fan, Y.X. Guo, H.R. Xue, J.P. He, J. Phys. Chem. C 117 (2013) 16896–16906.
[12] L. Calvillo, V. Celorrio, R. Moliner, M.J. Lázaro, Mater. Chem. Phys. 127 (2011) 335–341.
[13] Y. Shao, J. Liu, Y. Wang, Y. Lin, J. Mater. Chem. 19 (2009) 46–59.
[14] W. Yuan, Y. Cheng, P.K. Shen, C.M. Li, S.P. Jiang, J. Mater. Chem. A 3 (2015) 1961–1971.
[15] Y. Chen, J. Xu, X. Liu, Y. Tang, T. Lu, Appl. Catal. B: Environ. 140 (2013) 552–558.
[16] H.C. Chen, F.G. Sun, J.T. Wang, W.C. Li, W.M. Qiao, L.C. Ling, D.H. Long, J. Phys. Chem. C 117 (2013) 8318–8328.
[17] J.C. Calderona, G. Garcia, L. Calvillo, J.L. Rodriguez, M.J. Lazaro, E. Pastor, Appl. Catal. B: Environ. 165 (2015) 676–686.
[18] G.H. An, H.J. Ahn, ECS Solid State Lett. 3 (2014) M29–M32.
[19] H. Feng, Y. Liu, J. Li, Chem. Commun. 51 (2015) 2418–2420.
[20] S.H. Liu, S.C. Chen, W.H. Sie, Int. J. Hydrog. Energy 36 (2011) 15060–15067.
[21] C.D. Dong, C.W. Chen, C.F. Chen, C.M. Hung, Sci. Rep. 4 (2014).
[22] C.S. Chen, Y.T. Lai, T.C. Chen, C.H. Chen, J.F. Lee, C.W. Hsu, H.M. Kao, Nanoscale 6 (2014) 12644–12654.
[23] R. Zolfaghari, F.I.-R. Ahmadun, M.R. Othman, W.R.W. Daud, M. Ismail, Mater. Chem. Phys. 139 (2013) 262–269.
[24] K. Wang, Y. Wang, Z. Liang, Y. Liang, D. Wu, S. Song, P. Tsiakaras, Appl. Catal. B: Environ. 147 (2014) 518–525.
[25] T.Q. Lin, I.W. Chen, F.X. Liu, C.Y. Yang, H. Bi, F.F. Xu, F.Q. Huang, Science 350 (2015) 1508–1513.
[26] G.F. Long, K. Wan, M.Y. Liu, X.H. Li, Z.X. Liang, J.H. Piao, Chin. J. Catal. 36 (2015) 1197–1204.
[27] K. Wan, Z.P. Yu, Z.X. Liang, Catalysts 5 (2015) 1034–1045.
[28] X. Li, H. Wang, J.T. Robinson, H. Sanchez, G. Diankov, H. Dai, J. Am. Chem. Soc. 131 (2009) 15939–15944.
[29] R.I. Jafri, N. Rajalakshmi, S. Ramaprabhu, J. Mater. Chem. 20 (2010) 7114–7117.
[30] Y.Y. Shao, J.H. Sui, G.P. Yin, Y.Z. Gao, Appl. Catal. B: Environ. 79 (2008) 89–99.
[31] J.J. Zhang, Z.B. Wang, C. Li, L. Zhao, J. Liu, L.M. Zhang, D.M. Gu, J. Power Sources 289 (2015) 63–70.
[32] J. Zhu, G. He, L. Liang, Q. Wan, P.K. Shen, Electrochim. Acta 158 (2015) 374–382.
[33] Y. Li, W. Gao, L. Ci, C. Wang, P.M. Ajayan, Carbon 48 (2010) 1124–1130.
[34] L. Zhang, A. Gao, Y. Liu, Y. Wang, J. Ma, Electrochim. Acta 132 (2014) 416–422.
[35] V. Di Noto, E. Negro, J. Power Sources 195 (2010) 638–648.
[36] J.B. Zhu, M.L. Xiao, X. Zhao, K. Li, C.P. Liu, W. Xing, Chem. Commun. 50 (2014) 12201–12203.
[37] J.C. Calderón, G. García, L. Calvillo, J.L. Rodríguez, M.J. Lázaro, E. Pastor, Appl. Catal. B: Environ. 165 (2015) 676–686.
[38] J. Cao, X. Yin, L. Wang, M. Guo, J. Xu, Z. Chen, Int. J. Hydrog. Energy 40 (2015) 2971–2978.
[39] Q. Li, H. Pan, D. Higgins, R. Cao, G. Zhang, H. Lv, K. Wu, J. Cho, G. Wu, Small 11 (2015) 1443–1452.
[40] M. Veerapandian, S. Neethirajan, RSC Adv. 5 (2015) 75015–75024.
[41] X.M. Ning, H. Yu, F. Peng, H.J. Wang, J. Catal. 325 (2015) 136–144.
[42] E. Bayram, G. Yilmaz, S. Mukerjee, Appl. Catal. B: Environ. 192 (2016) 26–34.
[43] K. Wan, M.Y. Liu, Z.P. Yu, Z.X. Liang, Q.B. Liu, J.H. Piao, Y.Y. Zheng, Int. J. Hydrog. Energy 41 (2016) 18027–18032.
[44] Q. Han, B. Wang, Y. Zhao, C. Hu, L. Qu, Angew. Chem. Int. Ed. 54 (2015) 11433–11437.
[45] J.K. Dombrovskis, H.Y. Jeong, K. Fossum, O. Terasaki, A.E.C. Palmqvist, Chem. Mater. 25 (2013) 856–861.
[46] K.T. Lee, X.L. Ji, M. Rault, L.F. Nazar, Angew. Chem. Int. Ed. 48 (2009) 5661–5665.
[47] R. Silva, D. Voiry, M. Chhowalla, T. Asefa, J. Am. Chem. Soc. 135 (2013) 7823–7826.
[48] K. Wan, G.F. Long, M.Y. Liu, L. Du, Z.X. Liang, P. Tsiakaras, Appl. Catal. B: Environ. 165 (2015) 566–571.
[49] X.Q. Wang, J.S. Lee, Q. Zhu, J. Liu, Y. Wang, S. Dai, Chem. Mater. 22 (2010) 2178–2180.
[50] D.S. Yang, D. Bhattacharjya, S. Inamdar, J. Park, J.S. Yu, J. Am. Chem. Soc. 134 (2012) 16127–16130.
[51] D.Y. Zhao, J.L. Feng, Q.S. Huo, N. Melosh, G.H. Fredrickson, B.F. Chmelka, G.D. Stucky, Science 279 (1998) 548–552.
[52] R. Ryoo, S.H. Joo, S. Jun, J. Phys. Chem. B 103 (1999) 7743–7746.
[53] K. Wan, Z.P. Yu, Q.B. Liu, J.H. Piao, Y.Y. Zheng, Z.X. Liang, RSC Adv. 6 (2016) 75058–75062.
[54] W. Li, C. Liang, C. Liang, J. Qiu, Z. Zhou, G. Sun, Q. Xin, J. Phys. Chem. B 107 (2003) 6292–6299.
[55] K. Wan, Z. Yu, X. Li, M. Liu, G. Yang, J. Piao, Z. Liang, ACS Catal. 5 (2015) 4325–4332.
[56] F.B. Su, J.H. Zeng, X.Y. Bao, Y.S. Yu, J.Y. Lee, X.S. Zhao, Chem. Mater. 17 (2005) 3960–3967.
[57] Z. Zhang, J. Liu, J. Gu, L. Su, L. Cheng, Energy Environ. Sci. 7 (2014) 2535.
[58] J.R.C. Salgado, J.J. Quintana, L. Calvillo, M.J. Laí zaro, P.L. Cabot, I. Esparbe, E. Pastor, Phys. Chem. Chem. Phys. 10 (2008) 6796–6806.
[59] L. Wang, Y. Yamauchi, Chemistry 17 (2011) 8810–8815.